Genomic and transcriptomic landscape of advanced renal cell cancer to individualize treatment strategy

K. de Joode[¥1], W.S. van de Geer[¥1,2], G.J.L.H. van Leenders[3], P. Hamberg[4], H.M. Westgeest[5], A. Beeker[6], S.F. Oosting[7], J.M. van Rooijen[8], L.V. Beerepoot[9], M. Labots[10], R.H.J. Mathijssen[1], M.P. Lolkema[1,11], E. Cuppen[12,13], S. Sleijfer[1,11], H.J.G. van de Werken[×*2,14,15], A.A.M. van der Veldt[×*1,16]

[¥]Both authors contributed equally and are considered first author
[×]Both authors contributed equally and are considered last author
**Corresponding author*

[1]Department of Medical Oncology, Erasmus MC Cancer Institute, University Medical Center, Rotterdam, The Netherlands;
[2]Cancer Computational Biology Center, Erasmus MC Cancer Institute, University Medical Center, Rotterdam, The Netherlands;
[3]Department of Pathology, Erasmus MC, Rotterdam, the Netherlands;
[4]Department of Internal Medicine, Franciscus Gasthuis & Vlietland, Rotterdam, The Netherlands;
[5]Department of Internal Medicine, Amphia Hospital, Breda, The Netherlands;
[6]Department of Internal Medicine, Spaarne Gasthuis, Hoofddorp, The Netherlands;
[7]Department of Medical Oncology, University Medical Center Groningen, University of Groningen, Groningen, The Netherlands;
[8]Department of Internal Medicine, Martini Hospital, Groningen, The Netherlands;
[9]Department of Internal Medicine, Elisabeth-Tweesteden hospital, Tilburg, The Netherlands;
[10]Department of Medical Oncology, Amsterdam UMC, Vrije Universiteit Amsterdam, Department of Medical Oncology, Cancer Center Amsterdam, The Netherlands;
[11]Center for Personalized Cancer Treatment, Rotterdam, The Netherlands;
[12]Center for Molecular Medicine and Oncode Institute, University Medical Center Utrecht, Utrecht, The Netherlands;
[13]Hartwig Medical Foundation, Amsterdam, The Netherlands;
[14]Department of Urology, Erasmus MC Cancer Institute, University Medical Center, Rotterdam, The Netherlands;
[15]Department of Immunology, Erasmus MC Cancer Institute, University Medical Center, Rotterdam, The Netherlands;
[16]Departments of Radiology & Nuclear Medicine, Erasmus MC, Rotterdam, The Netherlands

<u>*Corresponding author(s)</u>
Astrid A.M. van der Veldt, Departments of Medical Oncology and Radiology & Nuclear Medicine, Erasmus MC Cancer Institute, Dr. Molewaterplein 40, 3015 GD Rotterdam, The Netherlands.
Tel: +31 (0)10 704 0 704. E-mail address: a.vanderveldt@erasmusmc.nl

Harmen J.G. van de Werken, Cancer Computational Bioldatogy Center, Erasmus MC Cancer Institute, Erasmus University Medical Center Rotterdam, Department of Immunology and Department of Urology, Internal Postal Address NA-1218-335, PO Box 2040, 3000 CA Rotterdam, the Netherlands.
Tel: +31 (0)10 703 1 829. Fax: +31 (0)10 704 4 731. E-mail address: h.vandewerken@erasmusmc.nl

Abstract

The genomic landscape of advanced renal cell cancer (RCC) was characterized for 91 patients to identify actionable targets and signatures by combining whole-genome sequencing (WGS) with matched RNA sequencing (RNA-Seq). WGS data were analyzed for somatic small variants, copy-number alterations (CNAs) and structural variants. Somatic aberrations were analyzed for driver genes, CNA drivers, mutational signatures, catastrophic events and fusion genes. For papillary and clear cell RCC, potential actionable drug targets were detected by WGS in 89% and 100% of the patients, respectively. RNA-Seq data of clear cell and papillary RCC were clustered according to a previously developed angio-immunogenic gene signature. WGS and RNA-Seq may improve therapeutic decision making for most patients with advanced RCC, including patients with non-clear cell RCC for whom no standard treatment is available to date. Prospective clinical trials are needed to evaluate the impact of genomic and transcriptomic diagnostics on survival outcome for advanced RCC patients.

54 ## Introduction

55 Renal cell carcinoma (RCC) consists of different histological subtypes [1,2]. The most common
56 histological subtype is clear cell RCC (ccRCC), accounting for approximately 75% of the RCC cases
57 [3]. The vast majority of ccRCC is characterized by the loss of the short arm of chromosome 3 (3p)[4],
58 which harbors several tumor suppressor genes. The function of these genes - *VHL*, *BAP1*, *PBRM1*,
59 and *SETD2* - is frequently inactivated due to additional somatic mutations or epigenetic changes
60 of these genes on the other allele [4,5]. Although these genetic aberrations can be observed in most
61 patients with ccRCC, the clinical behavior in individual patients differs significantly, from slowly
62 progressive disease over years to rapidly progressive disease with fast clinical deterioration.
63 Therefore, the management of advanced ccRCC varies from active surveillance to systemic
64 therapy.

65 In the past years, the therapeutic landscape for patients with advanced ccRCC has changed
66 significantly. The introduction of tyrosine kinase inhibitors (TKIs) [6,7], immune checkpoint
67 inhibitors (ICIs) [8,9], mammalian target of rapamycin (mTOR) inhibitors [10], and combinations of
68 these anti-cancer therapies [11-13], has significantly improved the outcome for patients with
69 advanced ccRCC. However, there are considerable interindividual differences in outcome, and
70 only a minority of patients experience durable responses [14]. For patients with advanced ccRCC,
71 treatment decision making is nowadays guided by the International Metastatic RCC Database
72 Consortium (IMDC) criteria [15-17]. These criteria include only clinical patient characteristics (i.e.
73 hemoglobin level, time from diagnosis to start of systemic therapy, Karnofsky performance state,
74 calcium level and neutrophil and platelets count).

75 Moreover, RCC with non-clear cell histology is a heterogeneous group of different subtypes, such
76 as papillary and chromophobe RCC [18]. As holds true for advanced ccRCC, the course of non-clear
77 cell RCC (nccRCC) differs significantly between patients [19,20]. Since the different nccRCC subtypes
78 are considered rare diseases, randomized phase three clinical trials are lacking for nccRCC [21]. As
79 a result, there is no clearly defined standard of care for patients with advanced nccRCC [20,22].

80 The development of RCC, including its metastatic potential and response to treatment, could
81 mainly be explained by the different genomics [2,4] and evolutionary pathways [5,23] of this disease.
82 Previous studies have focused on the molecular characterization of primary RCC [2,4,24] and the
83 genomic evolution of ccRCC [4,5,23]. For example, RNA expression analysis in ccRCC has identified
84 different immunogenic and angiogenic gene expression signatures [24,25], however, predictive
85 value for treatment efficacy has not been validated. To improve the individualized treatment
86 strategy and the survival outcomes for patients with ccRCC and nccRCC, more insight into the
87 genomic make-up of advanced RCC is required.

88 The objective of this study was to describe the genomic landscape of advanced RCC, by combining
89 whole-genome sequencing (WGS) with matched RNA sequencing (RNA-Seq) data. First, WGS was
90 applied to characterize the genomic make-up of RCC and to identify potential actionable targets
91 for systemic treatment in individual patients with ccRCC and nccRCC. Next, both WGS and
92 matched RNA-Seq data were combined for patients with ccRCC and papillary RCC (pRCC). The
93 RNA-Seq data were applied to cluster RCC based on immunogenic and angiogenic gene
94 expression patterns, aiming to identify those patients who could benefit from either treatment
95 with anti-angiogenic drugs, immunogenic drugs or a combination of these therapies.

96 ## Results

97 ### Patient selection

98 In total, WGS data from 91 patients with histopathologically confirmed RCC were included in the
99 analyses (**Figure 1A**). Additional RNA-Seq data were available for 28 patients (**Figure 1A**). Overall,
100 72 patients were diagnosed with ccRCC, nine patients with pRCC, one with chromophobe RCC,
101 one with tubulocystic RCC, and one with collecting duct carcinoma. For the remaining seven
102 patients with RCC, the subtype could not be further defined. The main biopsy sites were the
103 kidney (*N* = 24), bone (*N* = 15), and lymph nodes (*N* = 14) (**Figure 1B**). The median age of patients
104 at the time of biopsy was 65 years (range 40-83), 79% of the patients were male, and 78% of the
105 patients did not receive any systemic treatment before biopsy (**Table 1**). Most patients (84/91,
106 92%) were treated with systemic therapy after biopsy was collected. This treatment consisted
107 mostly of TKIs (61/84, 73%) or ICIs (19/84, 23%), whereas the remaining patients received
108 combination treatment (4/84, 5%). For 68 out of 84 (81%) patients, the first tumor response
109 (RECIST v1.1 [26]) to treatment (post tumor biopsy) could be established. Most patients had stable
110 disease (SD) (46%), followed by progressive disease (PD) (14%) and partial response (PR) (14%).

111

112

113

114 **Whole-genome sequencing analyses**

115 Somatic small variants, copy-number alterations (CNAs) and structural variants (SVs) were
116 identified as described previously [27]. The median tumor mutational burden (TMB) of patients
117 with ccRCC was 2.8 [interquartile range (IQR) 1.1] (**Figure 2A**). Only two patients (one with ccRCC
118 and one with undefined subtype of RCC) had a TMB > 10 [28]. In both these samples with high TMB,
119 mutational signatures were related to defective DNA mismatch repair, covering more than 25%
120 of their single-nucleotide variants (SNVs) (**Figure 2A/E**). Interestingly, the lowest TMB (i.e. 0.16)
121 was found in a patient with tubulocystic RCC (*N* = 1) who had very little genomic aberrations in
122 general, and only two detectable SVs (**Figure 2C/D;** tandem duplication and break-end). In the
123 total cohort, SBS40 (unknown etiology) was the dominant mutational signature, with a mean
124 relative contribution of 74%. To assess the reliability of the SBS40 calling, the mutational
125 signature calling was bootstrapped, which revealed a very high variance (median difference in
126 assignment of 37%) in the relative contribution of SBS40 (Supplementary figure 1).

127 The frequency of genomic SNVs, multi-nucleotide variants (MNVs), InDels, and the collective
128 coding mutations showed a similar pattern across the different RCC subtypes (Supplementary
129 figure 2, supplementary data file). In total, 713,077 somatically acquired SNVs, 173,579 InDels
130 and 9,964 MNVs were detected in the RCC genomes. Transversions were more frequently found
131 than transitions in ccRCC, pRCC and undefined subtypes (Supplementary figure 2B and 2E).
132 Missense variants were the most dominant protein variant type and accounted for > 60% of the
133 small variants in all subtypes (Supplementary figure 2G). The genome ploidy was mostly diploid,
134 and genome duplications were more frequent in ccRCC than in other subtypes (Supplementary
135 figure 2D). For 57% of ccRCC, the genome-wide ploidy was 2, while 32% had a genome doubling

136 with a ploidy of 3 or higher. Differences in DNA ploidy have been associated with tumor
137 differentiation and diploidy has been related to well-differentiated RCC [29]. Considering SVs, a
138 total of 3,121 deletions, 941 translocations, 2,196 tandem duplications, 4 insertions, 2,714
139 inversions and 641 break-ends were detected (Supplementary Fig 2F). When comparing the
140 mutational frequencies of ccRCC in our cohort to those in the TRACERx WGS cohort, a multicenter
141 prospective study analyzing the evolutionary features of ccRCC [5], the number of substitutions
142 was similar in both cohorts (7,224, Q1–Q3: [5648-8581] *vs*. 7,050, Q1–Q3: [6434-9504], *p*-value
143 = 0.45). The number of patients with events considered as chromothripsis was limited and
144 present in only five patients with ccRCC, two patients with pRCC and absent in the other subtypes.
145 Furthermore, these chromothriptic events mostly did not involve the classic t(3;5) event. Only
146 one of the samples with chromothripsis did have a t(3;5) translocation (Supplementary figure 3),
147 while these specific translocations were more frequently detected in the cohort of patients
148 without chromothriptic events (29.7%, Supplementary figure 4).

149 Next, the WGS data were analyzed on driver genes of the ccRCC samples using the dN/dS
150 algorithm and on CNAs by GISTIC 2.0. These driver gene analyses revealed that most driver genes
151 in ccRCC encompassed variations in the chromosome 3p region: *SETD2* (88.9%), *VHL* (73.6%),
152 *PBRM1* (61.1%), and *BAP1* (16.7%) together with mutations in tumor suppressor genes on other
153 chromosomes, such as *CDKN2A* (68.1%) and *PTEN* (16.7%) (**Figure 3,** supplementary data file). In
154 addition, a substantial number of patients with ccRCC had focal deletions in genes described as
155 possible tumor suppressor genes, e.g. *PTPRD* (59.7%) and *NEGR1* (36.1%) [4,30]. Deletions of *PTPRD*
156 have been described as a possible risk factor for the development of ccRCC [30,31]. Moreover,
157 amplifications were present in genes associated with cell proliferation and angiogenesis, such as

158 *CDK6* (55.6%) and *CCNE1* (19.4%) [32,33]. In total, pathogenic germline mutations related to cancer
159 or Von Hippel-Lindau syndrome were found in nine patients in different RCC subtypes and
160 included *ATM, FLCN, CHEK2, FH, SDHA* and *MITF* (**Figure 3**).

161 In addition, genes which were previously described as frequently mutated somatically (*q*-value <
162 0.05) in (cc)RCC by Braun *et al*. [34] and in pRCC by Turajlic *et al*. [35], that were not statistically
163 significant in our driver gene analysis, were included to extend our analysis. Nevertheless, many
164 of these added genes showed a low mutational frequency in our cohort, similarly for genes
165 associated with poor prognosis ccRCC [4], such as the Krebs cycle genes (e.g. *SDHA*, *FH*).

166 Furthermore, previously validated fusion events [36] were detected, with *CLTC-VMP1* and *SFPQ-*
167 *TFE3* both occurring once in the ccRCC group, along with a fusion event of *ASPSCR1-TFE3* in one
168 patient with pRCC. For both patients with a detected *TFE3* fusion, the histopathological diagnosis
169 had to be reconsidered. As a result, these patients were re-allocated in a different subcategory
170 of RCC, i.e. MiT family translocation renal cell carcinomas [1]. The previously described *TERT*
171 promoter hotspot variant (C228T) [5] was found in both ccRCC (*N* = 10) and pRCC (*N* = 2). Overall,
172 characteristic clear cell driver gene events — such as somatic *VHL* mutations/deletions — were
173 absent in nccRCC, except for *CDKN2A* deletions in pRCC.

174 In patients with ccRCC, both previously described and novel amplifications and deletions were
175 detected. Statistically significant CNA peaks and arm-level copy-number alterations in ccRCC are
176 presented in Supplementary figure 5. Previously described arm-level CNAs [37] included
177 amplifications of 1q, 5q, 7q, 8q, 12p and 20q, and deletions in 3p, 9p and 14q. Furthermore, in
178 the current cohort, amplifications of 5p, 7p, 12q, 16p and 20p, and deletions of 4p, 6p, 9q, 14p,

179 18p and 18q were also statistically significant. Next, we investigated if the tumors contained
180 targetable variants (**Figure 4**), which showed that most patients with RCC had one or more
181 variants indicated as potential targets or biomarkers for treatment. For example, for target-
182 specific variants encoded by *CDK4/6* or *EGFR*, specific drugs have been developed for other
183 cancer types [38-40]. This may result in off-label availability of these drugs for patients with similar
184 aberrations in RCC, e.g. in context of a clinical trial [41]. Furthermore, somatic aberrations in cancer
185 genes, e.g. *TP53*, are also considered biomarkers for targeted treatments [42]. Lastly, some variants
186 leading to specific mechanisms were also considered as targetable for treatment. For instance,
187 TKIs targeting VEGF signaling are known to be effective in patients with *VHL* mutations and are
188 on-label available for patients with RCC [43]. Overall, for the majority (96%) of patients in this cohort
189 actionable targets were detected, even for patients with nccRCC for whom no standard
190 treatment is available to date.

191 **Transcriptome analyses of advanced RCC**

192 Differential Expression Analysis (DEA) was performed on RNA-Seq data to discriminate the two
193 most frequently diagnosed histological subtypes, ccRCC (N = 24) and pRCC (N = 4). Next to the *t*-
194 distributed stochastic neighbor embedding (*t*-SNE), which showed a clear separation between
195 the two subtypes (Supplementary figure 6), the DEA resulted in 1,546 significantly (adjusted *p*-
196 value < 0.05) differentially expressed genes. The hundred genes with the smallest adjusted *p*-
197 value are shown in **Figure 5A.** In this top hundred list, several genes are known to be associated
198 with the development or course of RCC. For instance, *LOX* [44] and *MAPKAPK3* [45] correlate with
199 poor survival in RCC. In addition, various other genes were differentially expressed and have been
200 described in other malignancies, such as *TUSC2* [46], *CAPN1* [47], *PCSK6* [48], and *CD2* [49]. The differential

201 expression of these genes confirmed a clear distinction of pRCC and ccRCC at the transcriptomic
202 level.

203 Second, the pathway analysis (**Figure 5B**) of the significant differentially expressed genes
204 revealed cancer hallmarks such as oxidative phosphorylation and epithelial-mesenchymal
205 transition (EMT), among others [50]. Significant Reactome pathways [51] of differentially expressed
206 genes in ccRCC compared to pRCC samples, mainly showed pathways related to VEGF and
207 collagen formation. Pathways related to poor prognosis [4], such as the AMPK complex, the Krebs
208 cycle genes, the pentose phosphate pathway and fatty acid synthesis, were not found to be
209 differentially expressed between ccRCC and pRCC. A heatmap of the top differentially expressed
210 genes between ccRCC and pRCC and a *t*-SNE plot show that RCC samples of undefined subtype
211 cluster with either ccRCC or pRCC samples based on the differential gene expression of these
212 subtypes (Supplementary figure 7).

213 The 66 gene-signature has been based on previous data from the IMmotion150 trial [25]. High
214 expression of 'angiogenic' genes and certain 'invasion' genes is applied to sub-classify RCC as
215 'angiogenic', which would be predictive for response to TKIs targeting VEGF signaling. In case of
216 high expression in 'Ca^{2+}-Flux', 'T-Effector', and other 'invasion' genes, RCC is sub-classified as
217 'immunogenic', indicating a response to ICIs is likely. According to this gene signature, ccRCC
218 cases in the current cohort could be classified as either immunogenic or angiogenic (**Figure 5C**).
219 Moreover, all patients with pRCC had low expression of these genes, except for one individual
220 patient with expression in *EDNRB* [52].

221

222 ## Discussion

223 In this study, the genomic and transcriptomic landscape of advanced RCC was characterized for
224 91 individual patients. First, genomic data showed that, next to *VHL* mutations (73.6%), most
225 common driver gene mutations in ccRCC included alterations in tumor suppressor genes of
226 different pathways such as *SETD2* (88.9%) and *PTEN* (16.7%). While TMB was comparable
227 amongst the different subtypes of RCC, the driver gene analyses showed a distinctive pattern
228 between patients with ccRCC and nccRCC. Furthermore, WGS revealed potential actionable
229 targets for 87 out of 91 patients and WGS might therefore contribute to a more individualized
230 treatment strategy for patients with advanced RCC.

231 For a subgroup of patients (*N* = 28), transcriptomic data were also available. RNA-Seq
232 could be applied to distinguish ccRCC, pRCC and histologically undefined RCC based on the
233 differential gene expression. The application of the 66-gene signature [25] on the RNA-Seq data,
234 made it possible to sub-categorize ccRCC into immunogenic or angiogenic signatures, whereas
235 classification in pRCC using these signatures was not feasible.

236

237 At genomic level, the findings for ccRCC corresponded mostly with previous findings [4,5,53]. The
238 massive contribution of SBS40 to the mutational landscape of nearly all RCC subtypes in this
239 cohort is remarkable. However, bootstrapping showed that SBS40 was the least robust signature,
240 indicating that this signature could act as a sink for mutations that are difficult to fit. Since CPCT-
241 02 cohorts with other tumor types did not show the high contribution of SBS40 [54,55], this is most
242 certainly not a result of a bias in the sequencing or in our workflows. In contrast to other studies,
243 the number of chromothriptic events was limited in this study and occurred in only five patients

244 with ccRCC. In previous studies, chromothripsis was defined as the combination of a
245 chromothriptic event together with a translocation event with concurrent 3p loss and 5q gain,
246 which were called "t(3;5) chromothripsis events" [5]. Although both chromothriptic and
247 translocation (t(3;5)) events occurred in our cohort, for most of the cases these events were
248 independent of each other (Supplementary figure 3 and 4).

249 At transcriptomic level, assigning ccRCC biopsies into either immunogenic or angiogenic
250 signatures may indicate which treatment could be most beneficial for individual patients. The
251 introduction of ICIs has significantly changed the therapeutic landscape for patients with
252 advanced ccRCC [56,57], resulting in a clinical need to select patients who will benefit either from
253 angiogenic or immunogenic treatment [17]. These data could assist clinical decision making when
254 choosing the optimal treatment strategy for the individual patient with advanced ccRCC. For
255 patients with high expression of genes annotated as immunogenic, first–line treatment with ICIs
256 should be considered, whereas for patients with high expression in angiogenic genes treatment
257 with a TKI should be taken into consideration. For those patients with low expression throughout
258 all these genes, combination treatment with TKI/ICI may be considered, although treatment
259 based on actionable targets identified by WGS could be the most effective option. Treatment
260 selection based on gene expression has already shown promising results for patients with RCC
261 [12,58], however, further research in a prospective setting is still warranted [59].

262

263 The distinctive mutational gene pattern between ccRCC and nccRCC clearly showed that these
264 tumors are different entities, while differences within the nccRCC subtypes were also evident.
265 For example, none of the patients with nccRCC had somatic *VHL* mutations and also other ccRCC

266 driver genes hardly showed mutations in nccRCC. This is of great importance, as the development
267 of targeted drugs is based on driver mutations or consequences downstream. For instance, the
268 frequently mutated *VHL* gene in ccRCC has been the basis for the development of angiogenesis
269 inhibitors for this disease. The mutations in this tumor-suppressor gene result in the
270 accumulation of *HIF1α/2α*, eventually leading to overexpression of *VEGF/PDGF*, *AXL*, and *MET,*
271 among others [43,60]. Several TKIs that have been approved for the treatment of advanced ccRCC
272 [6,7,43,61] interfere at different levels in this cascade [43,60]. More recently, Hypoxia Inducible Factor
273 (HIF) inhibition has also shown proven efficacy in patients with *VHL* mutations [62]. However, as
274 patients with nccRCC in our cohort showed no mutations in *VHL* or other related pathways, it is
275 questionable whether treatment directed against the *VHL* pathway would be the most effective
276 therapy for this particular group of patients.
277
278 In clinical practice, RCC is usually defined histopathologically. As a result, there is a large
279 dependency on experienced pathologists. However, discrepancies among these experts remain
280 [63,64]. In our cohort, nearly 8% of RCC cases could not be sub-classified through histopathological
281 assessment. Thereby, for two patients a fusion gene was detected by WGS which led to revision
282 of the original histological diagnosis and allocation to a different subgroup, i.e. MiT family
283 translocation renal cell carcinoma [1]. As the histopathological classification defines the treatment
284 strategy, this could have significant clinical impact. Since different subtypes and growth patterns
285 of RCC are driven by gene expression [65], a next generation sequencing-based classifier could be
286 feasible. Here, we showed that analyses of driver mutations (*VHL*, *PBRM1*, *SETD2)* and RNA-Seq
287 data reveal clear differences among the different RCC subtypes. As shown in Supplementary

288 Figures 6 and 7, clustering of the undefined RCC subtypes is feasible and could be useful to clarify
289 the histological subtype in clinical practice.
290
291 This study has some important limitations. First, the collected clinical data within the CPCT-02
292 study were limited. For instance, only the first tumor response (according to RECIST v1.1.) after
293 biopsy was available and the response rates in this cohort were relatively low when compared to
294 the clinical trials. On one hand, these lower tumor response rates could be due to the
295 unavailability of ICIs, as patients were included between 2016 and 2019, when ICIs were not yet
296 available in first-line setting for RCC in the Netherlands. In addition, patients within the CPCT-02
297 study were treated in a real-world setting, which is known for its lower response rates compared
298 to response rates of clinical trials. In addition, due to the limited clinical data collection, it was
299 not possible to reliably correlate genomic and transcriptomic findings to clinical data. A
300 correlation with clinical data could have confirmed whether patients with certain gene signatures
301 indeed had benefit from a specific treatment. Therefore, validation in a prospective trial is
302 needed prior to clinical implementation.
303 Second, the limited number of patients with nccRCC made it challenging to run separate
304 analyses for this group. Since the subgroup of patients with nccRCC consists of different less
305 common and heterogeneous subtypes, and very little is known about the genomics of nccRCC.
306 Therefore, we decided to include all patients with nccRCC, even subgroups containing only a
307 single patient. Finally, the collected data were heterogeneous. For instance, not only biopsies of
308 metastases, but also biopsies from the kidney (including primary tumors) were included for the
309 analyses. However, it is not conceivable that this has significantly impacted the analysis, since

310 previous studies have shown clear consistencies between primary tumors and their metastasis [5].
311 In addition, the heterogeneity in this cohort reflects daily clinical practice of patients who present
312 with advanced RCC, including primary metastatic disease. Despite this clinical heterogeneity, a
313 clear genomic and transcriptomic signal could be extracted, indicating that the genomic and
314 transcriptomic analyses are feasible for clinical implementation.
315
316 In conclusion, there are evident genomic and transcriptomic differences between RCC subtypes.
317 The analysis of driver mutations, in combination with clustering of RNA-Seq data, could assist the
318 histopathological subtyping of RCCs in clinical practice. In addition, RNA-Seq data could identify
319 patients with ccRCC who may benefit more from treatment with either ICIs, TKIs or a combination
320 of these drugs. Genomic and transcriptomic analyses are promising to identify actionable targets
321 and to individualize treatment strategies in the majority of patients with RCC, even for patients
322 with nccRCC. Although these results are promising, prospective clinical trials are still needed to
323 evaluate whether genomic and transcriptomic diagnostics indeed contribute to improved
324 survival outcomes in individual patients with advanced RCC.
325

326 ## Materials and Methods

327 **Center for Personalized Medicine: Patient cohort, study procedures, sample collection, clinical**
328 **data**

329 In accordance with the Declaration of Helsinki, all patients within this study provided written
330 informed consent for participation in the Center for Personalized Cancer Treatment (CPCT-02)
331 study (NCT01855477) before study procedures started. The CPCT-02 study was approved by the
332 medical ethical committee of the University Medical Center Utrecht, as well as the Netherlands
333 Cancer Institute and local approval was provided for each participating site. Details regarding
334 inclusion criteria, the study protocol, sampling, and sequencing have been previously described
335 [27]. In summary, core needle biopsies from the tumor lesion, peripheral whole blood samples and
336 clinical data were collected across hospitals in the Netherlands. The response to treatment was
337 determined according to RECIST v1.1 [26]. WGS data from 103 biopsies of 101 patients with
338 advanced RCC were made available. Only one sample per patient was selected for the genomic
339 analyses. When multiple biopsies of one patient were available, the sample covering the most
340 clinical information and/or the sample with the highest estimated tumor cell percentage was
341 selected. The selection resulted in 91 WGS samples (51 previously described by Priestley *et al.* [27])
342 and 35 RNA samples.

343 **Pathological diagnosis**

344 To confirm the histopathological diagnosis of RCC, pathology reports were requested via PALGA,
345 the nationwide network and registry of histo- and cytopathology in the Netherlands [66]. Slides and
346 tissue blocks were not available for pathological revision. Alternatively, the pathology reports
347 were reviewed by a genito-urinary pathologist (GvL) to determine whether the microscopic

348 description and immunohistochemistry were compatible with the original diagnosis. The
349 following subtypes were annotated: clear cell, papillary, chromophobe, tubulocystic, and
350 collecting duct carcinoma. Histopathologically confirmed RCC of which the subtype remained
351 unclear was categorized as undefined subtype.

352 **Whole genome sequencing and preprocessing**

353 Between the 8th of August 2016 and the 3rd of October 2019, tumor and whole-blood pairs were
354 whole-genome sequenced at the Hartwig Medical Foundation (HMF) central sequencing center.
355 A HiSeqX system was applied and 2 × 150 base read pairs were generated using standard settings
356 (Illumina, San Diego, CA, USA). Preprocessing was performed as described by Priestley *et al* [27].
357 Briefly, read pair mapping was performed using BWA-mem [67] to the reference genome GRCh37
358 (human) with subsequent systematic variant calling and several quality control and/or correction
359 steps. The Genome Rearrangement IDentification Software Suite (GRIDSS) [68] was used for
360 structural variant (SV) calling and LINX (v1.11) [68] for gene fusion event calling. Computational
361 ploidy estimation and copy-number (CN) assessment was performed using the PURPLE (PURity &
362 PLoidy Estimator) pipeline [68], estimating tumor purity and CN profile by combining B-allele
363 frequency (BAF), read depth, and SVs.

364 **Somatic variant annotation and filtering**

365 Somatic variants were determined using Strelka and provided by the HMF as part of the data
366 request. Variant Call Format (VCF) files with somatic variants were annotated based on GRCh37
367 with HUGO gene symbols, HGVS notations, gnomAD [69] frequencies using VEP [70] (database release
368 95, merged cache), with setting "--per_gene". Exclusively somatic single-nucleotide variants

369 (SNVs), small InDels, multi-nucleotide variants (MNVs) with ≥ 3 alternative read observations and
370 passing variant caller quality control were included in the analyses. Furthermore, population
371 variants were removed to prevent germline leakage, based on the gnomAD database (v2.0.2) [69]:
372 gnomAD exome (ALL) allele frequency ≥ 0.001; and gnomAD genome (ALL) ≥ 0.005. Variants
373 specific for the Dutch CPCT cohort were removed based on a panel-of-normals from 1,762
374 representative normal blood HMF samples. The most deleterious mutation was used to annotate
375 the overlapping gene for each sample.

376 **Tumor Mutational Burden calculation**

377 The number of mutations per megabase pair was calculated as the amount of somatic genome-
378 wide SNVs, MNVs, and InDels divided by the number of callable nucleotides in the human
379 reference genome (GRCh37) FASTA file:

380 $$TMB = \frac{\left(SNVs_g + MNVs_g + InDels_g\right)}{\left(\frac{2858674662}{10^6}\right)}$$

381 **Ploidy and copy-number analysis**

382 Broad and focal somatic CN alterations in ccRCC were identified by GISTIC2.0 [71] (v2.0.23), using
383 the following parameters: genegistic 1, gcm extreme, maxseg 4000, broad 1, brlen 0.98, conf
384 0.95, rx 0, cap 3, saveseg 0, armpeel 1, smallmem 0, res 0.01, ta 0.1, td 0.1, savedata 0, savegene
385 1, qvt 0.1. Distinction between shallow and deep CN events per region was based on thresholding
386 performed by GISTIC2.0. The alterations were assigned a score taking both the amplitude and
387 the frequency of its occurrence across samples into account (G-score). Thresholding was divided
388 into five CN categories; two for deletions (-2 = deep, possibly homozygous loss, -1 = shallow,

389 possibly heterozygous loss), one for diploid (0 = diploid) and two for amplifications (1 = few
390 additional copies, often broad gain, 2 = more copies, often focal gain). Annotation of GISTIC2.0
391 peaks was performed as follows: A) Wide peaks were annotated with all overlapping canonical
392 UCSC genes within the genomic limits of said peak. B) Focal peaks were annotated based on
393 overlapping genomic coordinates, using custom R scripts and UCSC gene annotations.

394 **Structural variant analysis**

395 SVs affecting genes were imported using custom R scripts, overlapping genes on at least one
396 breakpoint, using GRCh37 genomic coordinates. SVs with an upstream or downstream Tumor
397 Allele frequency (TAF) below 0.1 as determined by PURPLE and GRIDSS [68] were discarded along
398 with SVs that affected all exons of a gene. In the case of both (multiple) mutations and/or SVs in
399 the same gene, these were annotated as 'multiple mutations'.

400 **Fusion gene analysis**

401 WGS-based LINX TSV files were imported using R and overlapped with the three pillars of
402 ChimerDB [36]; deep sequencing data (ChimerSeq), text mining of PubMed publications
403 (ChimerPub), with extensive manual annotations (ChimerKB). Events that were not present in
404 any pillar of ChimerDB and intra-gene fusions were filtered out. RNA-Seq based fusion genes
405 detected with Isofox (https://github.com/hartwigmedical/hmftools/tree/master/isofox) were
406 imported using R and overlapped with the fusion events detected in the DNA sequencing.

407 **Somatic Driver Genes Analysis**

408 We utilized the dN/dS model (192 Poisson rate parameters; under the full trinucleotide model)
409 to identify genes undergoing mutational selection in the ccRCC patients with the R package

410 dndscv [72] (v0.0.1.0). Both the substitution model and InDel model were used and were corrected
411 for sequence composition, gene length and mutational signatures. These models test the ratio
412 between nonsynonymous (missense, nonsense and essential splice site) and background
413 (synonymous) mutations. To identify genes that drive selection, a *q*-value < 0.05 (both including
414 and excluding the InDel model) was used.

415 **Mutational signatures analysis**

416 Mutational signatures analysis was performed using the MutationalPatterns R package (v3.2.0)[73].
417 The mutational signatures based on single base substitutions (*N* = 90 v3 signatures) were
418 downloaded from COSMIC [74]. SNVs were categorized according to their respective trinucleotide
419 context (GRCh37) into a mutational spectrum matrix M_{ij} (where *i* represents 1:96 trinucleotide
420 contexts and *j* represents the number of 1:91 samples) and subsequently, a constrained linear
421 combination of the ninety mutational signatures was constructed per sample using non-negative
422 least squares regression implemented in the R package pracma (v2.2.9). Mutational signatures
423 were bootstrapped (*N* = 100) with MutationalPatterns and argument 'method' set to "strict" to
424 assess calling stability. Signature contribution for each sample was determined per 100
425 samplings, per signature.

426 **Chromothripsis**

427 Chromothripsis (CT), also known as chromosomal shattering, followed by seemingly random re-
428 ligation, was detected using Shatterseek [75] (v0.4) with default settings. The following definition
429 of CT was employed: (1) ≥25 intrachromosomal SVs involved in the event; (2) ≥7 oscillating CN
430 segments (2 CN states) or ≥14 oscillating CN segments (3 CN states); (3) CT event involving ≥20

431 Mb; (4) satisfying the test of equal distribution of SV types (*p*-value > 0.05); and (5) satisfying the
432 test of nonrandom SV distribution within the cluster region or chromosome (*p*-value ≤ 0.05).

433 **Actionable targets**

434 iClusion (https://iclusion.com) data, which connects specific or gene-level aberrations to clinical
435 cancer studies, were provided by HMF. This integrates clinical interpretations from Precision
436 Oncology Knowledge Base (OncoKB) [76], Clinical Interpretation of Variants in Cancer (CIViC) [77] and
437 Cancer Genome Interpreter (CGI) [78]. All targets and biomarkers were overlapped with filtered
438 molecular data to verify presence. Targets marked as "gene-level" were generalized for other
439 variation in those genes, not listed in the iClusion data. The identified targets were assessed and
440 manually categorized in the following three categories: on-label drugs for RCC, off-label available,
441 investigational drugs. Drugs were considered on-label when approval was given for any subtype
442 of RCC in the Netherlands. Whether drugs were on- or off-label available in the Netherlands is
443 defined by the Dutch Medicines Evaluation Board ("College ter Beoordeling van
444 Geneesmiddelen") [79]. This evaluation board takes previous approvals by the U.S. Food and Drug
445 Administration (FDA) and/or European Medicines Agency (EMA) in consideration.

446 **Germline analysis**

447 Known pathogenic germline variants (GRCh37) related to cancer and/or Von Hippel-Lindau
448 syndrome were retrieved from ClinVar [80] that were less than 51 bp long, with a review status of
449 "practice guideline", "expert panel", "multiple submitters" or "at least one star". These ClinVar
450 variants were used as filter for the import of germline variants from VCF files of our cohort.
451 Variants with at least 2 reads and passing variant caller quality control were included.

452 Furthermore, variants that were annotated with “high” impact, in genes with known germline
453 variation in RCC (*FH*, *SDHA*, *SDHB*, *SDHC*, *SDHD*, *TCEB1*, *FLCN*, *CHEK2*) were included.

454 **RNA sequencing**

455 RNA was isolated from biopsy using the QIAsymphony RNA Kit (Qiagen, Hilden, Germany) for
456 tissue and quantified on the Qubit. Between 50 and 100 ng of RNA was used as input for the
457 KAPA RNA HyperPrep Kit with RiboErase (Human/Mouse/Rat) library preparation (Roche) on an
458 automated liquid handling platform (Beckman Coulter). RNA was fragmented (high temperature
459 in the presence of magnesium) to a target length of 300 bp. Barcoded libraries were sequenced
460 as pools on either a NextSeq 500 (V2.5 reagents) generating 2 x 75 base read pairs or on a
461 NovaSeq 6000 generating 2 x 150 base read pairs using standard settings (Illumina, San Diego,
462 CA, USA). BCL output from the sequencing platform was converted to FASTQ using Illumina’s
463 bcl2fastq tool (versions 2.17 to 2.20) using default parameters. RNA-Seq data was aligned using
464 STAR [81] to GRCh37 resulting in unsorted BAMs including chimeric reads as output. Gene and
465 transcript counts were generated and used for subsequent fusion detection using Isofox
466 (https://github.com/hartwigmedical/hmftools/tree/master/isofox).

467 **RNA sequencing analyses**

468 Raw read counts were imported in R and filtered on protein coding genes based on Ensembl GTF
469 file [82] (Homo sapiens GRCh37, version 87). *t*-distributed stochastic neighbor embedding (*t*-SNE)
470 was performed on variance stabilized read counts (generated by DESeq2
471 varianceStabilizingTransformation) of all protein coding genes. Differential expression analysis
472 between ccRCC and pRCC was performed on raw read counts using DESeq2 [83] and the Wald-test.

473 Statistical significant results with Benjamini-Hochberg adjusted *p*-value < 0.05 were further
474 filtered to base mean > 100 counts and absolute $\log_2$ fold change ≥ 1. The heatmap with the top
475 most significantly differentially expressed genes (based on lowest adjusted *p*-value) was made
476 using variance stabilized read counts and euclidean distances on scaled data. Gene signature
477 heatmap was produced with centered Z-Scores with Euclidean distances. Gene set enrichment
478 analyses were performed using fgsea [84] (Monte Carlo approach with Adaptive Multilevel Splitting)
479 with MSigDB [85] Hallmarks and Reactome pathways [51] as gene sets. Reproduction of the D'Costa
480 *et al.* gene signature [25] was done using 65 of 66 original genes, since *PECAM1* was on a genome
481 patch not included in the RNA-Seq mapping supplied by HMF. Heatmaps were produced using
482 pheatmap with Ward.D clustering.

483 **Data and material availability**

484 Data was provided by HMF, which were used under data request number DR-088 for the current
485 study. Both WGS, RNA-Seq and clinical data are freely available for academic use from the HMF
486 through standardized procedures and request forms can be found at
487 https://www.hartwigmedicalfoundation.nl. All tools and scripts used for processing of the WGS
488 data are available at https://github.com/hartwigmedical/ and/or can be provided by authors
489 upon request.

490

491 **Tables**

492

493 **Table 1. Overview of patients' characteristics**

	Frequency	Percentage
Sex		
Male	**72**	**79%**
Female	**19**	**21%**
Median age 65 years [range 40-83]	---------	---------
Histological subtype		
Clear cell RCC (ccRCC)	**72**	**79%**
Non-clear cell RCC (nccRCC)	**12**	**13%**
Papillary RCC (pRCC)	9	75%
Chromophobe RCC (chRCC)	1	8%
Collecting duct carcinoma (CDC)	1	8%
Tubulocystic RCC (tRCC)	1	8%
Undefined subtype	**7**	**8%**
Prior treatment (n=number of lines)		
No	**71**	**78%**
Yes (1)	**10**	**11%**
Yes (≥2)	**10**	**11%**
Treatment after biopsy (N = 84)		
Tyrosine kinase inhibitors (TKIs)	**61**	**73%**
Pazopanib	36	59%
Sunitinib	23	38%
Cabozantinib	1	1.6%
Lenvatinib	1	1.6%
Immune checkpoint inhibitors (ICIs)	**19**	**23%**
Nivolumab monotherapy	13	68%
Nivolumab + ipilimumab	6	32%
Combination treatment	**4**	**5%**
Avelumab + axitinib	4	100%

494

495

496 ## Figure legends

497 **Figure 1 Overview of sample selection and biopsy sites**

498 **1A** illustrates the selection of samples for both the WGS (*N* = 91) and matched RNA-Seq (*N* = 28)
499 analyses. In **1B**, the main biopsy sites are shown. Next to the illustrated biopsy sites, other biopsy
500 sites (*N* = 20) include for instance biopsies from subcutaneous tissue. **1B** was created with
501 biorender.

502 **Figure 2 Overview of genomic characteristics of whole-genome sequenced advanced RCC**
503 **cohort (*N* = 91)**

504 Track **A** shows the tumor mutational burden (mutations per Mb; yellow for low (0-5), orange for
505 medium (5-10) and red for high (> 10)). Track **B** shows the mean genome-wide ploidy, with white
506 representing diploidy. Tracks **C** and **D** illustrate the abundance of structural variants and the
507 relative frequency of the types of these variants. Tracks **E** and **F** show the relative mutational
508 signature contribution (COSMIC signatures v3) and the relative frequency of mutational changes
509 at base level. Track **G** shows the presence of chromothripsis. Track **H** shows whether patients
510 were treatment naive at time of biopsy. Tracks **I** and **J** indicate the first treatment given after
511 biopsy (if any) and the first tumor response according to RECIST v1.1, respectively. On the x-axis
512 the figure is arranged in descending order by tumor mutational burden per RCC subtype. ccRCC
513 = clear cell renal cell carcinoma. pRCC = papillary renal cell carcinoma. Undefined subtype = renal
514 cell carcinoma, with undefined subtype. chRCC = chromophobe renal cell carcinoma. CDC =
515 collecting duct carcinoma. tRCC = tubulocystic renal cell carcinoma. NA = not available.

516 **Figure 3 Overview of coding mutations and copy-number alterations in driver genes in whole-**
517 **genome sequenced advanced renal cell carcinoma cohort (*N* = 91)**

518 The oncoplot in track **A** shows mutations (filled center) and copy-number alterations (grid cell
519 background) of driver genes determined by dN/dS and GISTIC2.0. Track **B** also shows an oncoplot,
520 but on selected genes, not passing any statistical threshold. Germline pathogenic mutations are
521 indicated with a capital letter 'G' (and red border), utilizing the same color coding as the somatic
522 mutations. Consequential fusion genes are indicated in yellow, with a red border. Track **C** shows
523 the tumor mutational burden (mutations per Mb; yellow for low (0-5), orange for medium (5-10)

524 and red for high (> 10)). Tracks **D**, **E** and **F** show whether patients were treatment naive at time of
525 biopsy, if systemic treatment was given after time of biopsy, and the first tumor response after
526 systemic treatment according to RECIST v1.1, respectively. Bold sample names with asterisks
527 indicate MiT family translocation RCC. Figure is arranged in descending order by tumor mutational
528 burden per RCC subtype on the x-axis.

529 **Figure 4 Overview of DNA-based biomarkers and potential treatment options in the whole-**
530 **genome sequenced advanced renal cell carcinoma cohort (*N* = 91)**
531 Track **A** Percentage of potential available treatment options based on genomic characteristics.
532 Treatment options are categorized according to the highest level of drug availability in clinical
533 practice (on label available – off label available – investigational drugs). Track **B** Potentially
534 actionable alterations at gene-level with each column representing a sample, ordered
535 descendingly by tumor mutational burden per subtype on the x-axis. Detailed description of
536 actionable targets can be found in Supplementary Data file 1.

537 **Figure 5 RNA sequencing cohort and differential expression analysis between clear cell renal**
538 **cell carcinoma (ccRCC) and papillary RCC (pRCC) with classification according to gene**
539 **signatures[25]**
540 Track **A** shows a heatmap of Z-scores of variance stabilized values with unsupervised clustering of
541 the top 100 transcripts based on smallest adjusted *p*-value and colored according to Z-scores.
542 Tracks **B** shows gene set enrichments based on sets (y-axis) from the molecular signatures
543 database hallmarks and Reactome pathways, with the normalized enrichment score (NES) on the
544 x-axis. Bar charts are visualized with ccRCC taken as reference (*N* = 24) (positive NES equals
545 expression up in ccRCC and down in pRCC (*N* = 4)). Track **C** shows unsupervised clustering on the
546 rows (patients) with color coding indicating the RCC subtype (purple for ccRCC and pink for pRCC)
547 and colored according to Z-scores. The x-axis has been cut into several gene groups related to
548 angiogenesis, invasion, Ca^{2+}-flux and T-effector cells, as defined by D'Costa *et al*. [25] and by their
549 stated order.

550
551

Acknowledgements

This publication and the underlying study have been made possible partly on the basis of the data that Hartwig Medical Foundation and the Center of Personalized Cancer Treatment (CPCT) have made available to the study. Furthermore, we would like to thank the nationwide network and registry of histo- and cytopathology in the Netherlands (PALGA) for their assistance on retrieving and storing the pathological records of the included patients with RCC. Figure 1 was created with BioRender (https://biorender.com/).

Author contributions

K.J., W.S.G., H.J.G.W. and A.A.M.V. wrote the manuscript which all authors have reviewed critically. W.S.G. and H.J.G.W. performed the bioinformatical analyses. K.J. and A.A.M.V. assessed the clinical data. G.J.L.H.L. reviewed and assessed the histopathological data. P.H., H.M.W., A.B., S.F.O, J.M.R., L.V.B., M.L. and R.H.J.M. are clinical contributors. M.P.L. and S.S. participated in the board of the CPCT-02 study. E.C. coordinated the sequencing of samples and contributed to the bioinformatical analyses.

Conflicts of interest

P.H. declares consultancy roles for Astellas, MSD, Ipsen, Pfizer, AstraZeneca, and Bristol-Myers Squibb, all outside the submitted work; H.M.W. declares honoraria from Roche and Astellas and travel expenses from Ipsen and Astellas, all outside the submitted work; S.F.O declares research grants from Novartis, Pfizer and Celldex Therapeutics and advisory board for Bristol Myers Squibb (all paid to the institution); M.L. declares speakers fee of BMS and advisory board of MSD, both paid to institution; R.H.J.M. declares speakers fee from Novartis and advisory role for Servier, patency from Pamgene, and investigator-initiated research (paid to institution) from Astellas, Bayer, Boehringer-Ingelheim, Cristal Therapeutics, Pamgene, Pfizer, Novartis, Roche, Sanofi, Servier, all outside the submitted work; M.P.L. declares advisory board for Amgen, Astellas, Astra Zeneca, Bayer, INCa, Janssen Cilag BV, MSD, Novartis, Pfizer, Roche, Sanofi, Servier, consulting role for Julius Clinical and Research Grants (paid to institution) from Astellas, Janssen, MSD, Sanofi, all outside the submitted work; H.J.G.W. declares speakers honoraria from Bayer,

580 Depositary receipts for shares from Cergentis B.V. all outside the submitted work; A.A.M.V.
581 reports advisory board (all paid to institution) of BMS, MSD, Merck, Pfizer, Ipsen, Eisai, Pierre
582 Fabre, Roche, Novartis, Sanofi, all outside the submitted work. All other authors declare no
583 competing interests.

584 **References**

585 1. Moch, H., Cubilla, A.L., Humphrey, P.A., Reuter, V.E. & Ulbright, T.M. The 2016 WHO
586 Classification of Tumours of the Urinary System and Male Genital Organs-Part A: Renal, Penile,
587 and Testicular Tumours. *Eur Urol* **70**, 93-105 (2016).
588 2. Cancer Genome Atlas Research, N. *et al.* Comprehensive Molecular Characterization of Papillary
589 Renal-Cell Carcinoma. *N Engl J Med* **374**, 135-45 (2016).
590 3. Padala, S.A. *et al.* Epidemiology of Renal Cell Carcinoma. *World J Oncol* **11**, 79-87 (2020).
591 4. Cancer Genome Atlas Research, N. Comprehensive molecular characterization of clear cell renal
592 cell carcinoma. *Nature* **499**, 43-9 (2013).
593 5. Mitchell, T.J. *et al.* Timing the Landmark Events in the Evolution of Clear Cell Renal Cell Cancer:
594 TRACERx Renal. *Cell* **173**, 611-623 e17 (2018).
595 6. Motzer, R.J. *et al.* Sunitinib versus interferon alfa in metastatic renal-cell carcinoma. *N Engl J*
596 *Med* **356**, 115-24 (2007).
597 7. Mendez-Vidal, M.J. *et al.* Pazopanib: Evidence review and clinical practice in the management of
598 advanced renal cell carcinoma. *BMC Pharmacol Toxicol* **19**, 77 (2018).
599 8. Motzer, R.J. *et al.* Nivolumab versus Everolimus in Advanced Renal-Cell Carcinoma. *N Engl J Med*
600 **373**, 1803-13 (2015).
601 9. Motzer, R.J. *et al.* Nivolumab plus ipilimumab versus sunitinib in first-line treatment for
602 advanced renal cell carcinoma: extended follow-up of efficacy and safety results from a
603 randomised, controlled, phase 3 trial. *Lancet Oncol* (2019).
604 10. Motzer, R.J. *et al.* Efficacy of everolimus in advanced renal cell carcinoma: a double-blind,
605 randomised, placebo-controlled phase III trial. *Lancet* **372**, 449-56 (2008).
606 11. Powles, T. *et al.* Pembrolizumab plus axitinib versus sunitinib monotherapy as first-line
607 treatment of advanced renal cell carcinoma (KEYNOTE-426): extended follow-up from a
608 randomised, open-label, phase 3 trial. *Lancet Oncol* **21**, 1563-1573 (2020).
609 12. Choueiri, T.K. *et al.* Updated efficacy results from the JAVELIN Renal 101 trial: first-line avelumab
610 plus axitinib versus sunitinib in patients with advanced renal cell carcinoma. *Ann Oncol* **31**, 1030-
611 1039 (2020).
612 13. Rini, B.I. *et al.* Atezolizumab plus bevacizumab versus sunitinib in patients with previously
613 untreated metastatic renal cell carcinoma (IMmotion151): a multicentre, open-label, phase 3,
614 randomised controlled trial. *Lancet* **393**, 2404-2415 (2019).
615 14. Flippot, R., Escudier, B. & Albiges, L. Immune Checkpoint Inhibitors: Toward New Paradigms in
616 Renal Cell Carcinoma. *Drugs* **78**, 1443-1457 (2018).
617 15. Heng, D.Y. *et al.* External validation and comparison with other models of the International
618 Metastatic Renal-Cell Carcinoma Database Consortium prognostic model: a population-based
619 study. *Lancet Oncol* **14**, 141-8 (2013).
620 16. Guida, A. *et al.* Identification of international metastatic renal cell carcinoma database
621 consortium (IMDC) intermediate-risk subgroups in patients with metastatic clear-cell renal cell
622 carcinoma. *Oncotarget* **11**, 4582-4592 (2020).
623 17. Vano, Y.A. *et al.* First-Line Treatment of Metastatic Clear Cell Renal Cell Carcinoma: What Are
624 the Most Appropriate Combination Therapies? *Cancers (Basel)* **13**(2021).
625 18. Truong, L.D. & Shen, S.S. Immunohistochemical diagnosis of renal neoplasms. *Arch Pathol Lab*
626 *Med* **135**, 92-109 (2011).
627 19. Hong, B. *et al.* The Clinicopathological Features and Prognosis in Patients With Papillary Renal
628 Cell Carcinoma: A Multicenter Retrospective Study in Chinese Population. *Front Oncol* **11**,
629 753690 (2021).

630 20. Sepe, P. *et al.* Characteristics and Treatment Challenges of Non-Clear Cell Renal Cell Carcinoma.
631 *Cancers (Basel)* **13**(2021).
632 21. Powles, T. *et al.* ESMO Clinical Practice Guideline update on the use of immunotherapy in early
633 stage and advanced renal cell carcinoma. *Annals of Oncology* **32**, 1511-1519 (2021).
634 22. Osterman, C.K. & Rose, T.L. A Systematic Review of Systemic Treatment Options for Advanced
635 Non-Clear Cell Renal Cell Carcinoma. *Kidney Cancer* **4**, 15-27 (2020).
636 23. Turajlic, S. *et al.* Tracking Cancer Evolution Reveals Constrained Routes to Metastases: TRACERx
637 Renal. *Cell* **173**, 581-594 e12 (2018).
638 24. Ricketts, C.J. *et al.* The Cancer Genome Atlas Comprehensive Molecular Characterization of
639 Renal Cell Carcinoma. *Cell Rep* **23**, 313-326 e5 (2018).
640 25. D'Costa, N.M. *et al.* Identification of gene signature for treatment response to guide precision
641 oncology in clear-cell renal cell carcinoma. *Sci Rep* **10**, 2026 (2020).
642 26. Eisenhauer, E.A. *et al.* New response evaluation criteria in solid tumours: revised RECIST
643 guideline (version 1.1). *Eur J Cancer* **45**, 228-47 (2009).
644 27. Priestley, P. *et al.* Pan-cancer whole-genome analyses of metastatic solid tumours. *Nature* **575**,
645 210-216 (2019).
646 28. Alexandrov, L.B. *et al.* Signatures of mutational processes in human cancer. *Nature* **500**, 415-21
647 (2013).
648 29. Abou-Rebyeh, H., Borgmann, V., Nagel, R. & Al-Abadi, H. DNA ploidy is a valuable predictor for
649 prognosis of patients with resected renal cell carcinoma. *Cancer* **92**, 2280-5 (2001).
650 30. Ortiz, B., White, J.R., Wu, W.H. & Chan, T.A. Deletion of Ptprd and Cdkn2a cooperate to
651 accelerate tumorigenesis. *Oncotarget* **5**, 6976-82 (2014).
652 31. Du, Y. *et al.* Polymorphism in protein tyrosine phosphatase receptor delta is associated with the
653 risk of clear cell renal cell carcinoma. *Gene* **512**, 64-9 (2013).
654 32. Tadesse, S., Yu, M., Kumarasiri, M., Le, B.T. & Wang, S. Targeting CDK6 in cancer: State of the art
655 and new insights. *Cell Cycle* **14**, 3220-30 (2015).
656 33. Li, Y., Shen, Y., Zhu, Z., Wen, H. & Feng, C. Comprehensive analysis of copy number variance and
657 sensitivity to common targeted therapy in clear cell renal cell carcinoma: In silico analysis with in
658 vitro validation. *Cancer Med* **9**, 6020-6029 (2020).
659 34. Braun, D.A. *et al.* Interplay of somatic alterations and immune infiltration modulates response to
660 PD-1 blockade in advanced clear cell renal cell carcinoma. *Nat Med* **26**, 909-918 (2020).
661 35. Turajlic, S., Larkin, J. & Swanton, C. SnapShot: Renal Cell Carcinoma. *Cell* **163**, 1556-1556 e1
662 (2015).
663 36. Jang, Y.E. *et al.* ChimerDB 4.0: an updated and expanded database of fusion genes. *Nucleic Acids*
664 *Research* **48**, D817-D824 (2019).
665 37. Beroukhim, R. *et al.* Patterns of gene expression and copy-number alterations in von-hippel
666 lindau disease-associated and sporadic clear cell carcinoma of the kidney. *Cancer Res* **69**, 4674-
667 81 (2009).
668 38. Du, Z. *et al.* Structure-function analysis of oncogenic EGFR Kinase Domain Duplication reveals
669 insights into activation and a potential approach for therapeutic targeting. *Nat Commun* **12**,
670 1382 (2021).
671 39. Ho, G.F. *et al.* Real-world experience of first-line afatinib in patients with EGFR-mutant advanced
672 NSCLC: a multicenter observational study. *BMC Cancer* **19**, 896 (2019).
673 40. Braal, C.L. *et al.* Inhibiting CDK4/6 in Breast Cancer with Palbociclib, Ribociclib, and Abemaciclib:
674 Similarities and Differences. *Drugs* **81**, 317-331 (2021).
675 41. van der Velden, D.L. *et al.* The Drug Rediscovery protocol facilitates the expanded use of existing
676 anticancer drugs. *Nature* **574**, 127-131 (2019).

677 42. Zhu, G. *et al.* Mutant p53 in Cancer Progression and Targeted Therapies. *Front Oncol* **10**, 595187
678 (2020).
679 43. Alonso-Gordoa, T. *et al.* Targeting Tyrosine kinases in Renal Cell Carcinoma: "New Bullets against
680 Old Guys". *Int J Mol Sci* **20**(2019).
681 44. Lin, S. *et al.* Comprehensive analysis on the expression levels and prognostic values of LOX
682 family genes in kidney renal clear cell carcinoma. *Cancer Med* **9**, 8624-8638 (2020).
683 45. Oh, E. *et al.* Genome-Wide Transcriptomic Analysis of Non-Tumorigenic Tissues Reveals Aging-
684 Related Prognostic Markers and Drug Targets in Renal Cell Carcinoma. *Cancers (Basel)* **13**(2021).
685 46. Rimkus, T., Sirkisoon, S., Harrison, A. & Lo, H.W. Tumor suppressor candidate 2 (TUSC2, FUS-1)
686 and human cancers. *Discov Med* **23**, 325-330 (2017).
687 47. Pan, X.Q., Huang, W., Jin, L.W., Lin, H.Z. & Xu, X.Y. A Novel Pyroptosis-Related Prognostic
688 Signature for Risk Stratification and Clinical Prognosis in Clear Cell Renal Cell Carcinoma. *Dis*
689 *Markers* **2022**, 8093837 (2022).
690 48. Wang, P., Wang, F., Wang, L. & Pan, J. Proprotein convertase subtilisin/kexin type 6 activates the
691 extracellular signal-regulated kinase 1/2 and Wnt family member 3A pathways and promotes in
692 vitro proliferation, migration and invasion of breast cancer MDA-MB-231 cells. *Oncol Lett* **16**,
693 145-150 (2018).
694 49. Han, J. *et al.* MMP11 and CD2 as novel prognostic factors in hormone receptor-negative, HER2-
695 positive breast cancer. *Breast Cancer Res Treat* **164**, 41-56 (2017).
696 50. Ding, X.F., Zhou, J., Hu, Q.Y., Liu, S.C. & Chen, G. The tumor suppressor pVHL down-regulates
697 never-in-mitosis A-related kinase 8 via hypoxia-inducible factors to maintain cilia in human renal
698 cancer cells. *J Biol Chem* **290**, 1389-94 (2015).
699 51. Jassal, B. *et al.* The reactome pathway knowledgebase. *Nucleic Acids Res* **48**, D498-D503 (2020).
700 52. Wuttig, D. *et al.* CD31, EDNRB and TSPAN7 are promising prognostic markers in clear-cell renal
701 cell carcinoma revealed by genome-wide expression analyses of primary tumors and
702 metastases. *Int J Cancer* **131**, E693-704 (2012).
703 53. Carlo, M.I. *et al.* Prevalence of Germline Mutations in Cancer Susceptibility Genes in Patients
704 With Advanced Renal Cell Carcinoma. *JAMA Oncol* **4**, 1228-1235 (2018).
705 54. van Riet, J. *et al.* The genomic landscape of 85 advanced neuroendocrine neoplasms reveals
706 subtype-heterogeneity and potential therapeutic targets. *Nat Commun* **12**, 4612 (2021).
707 55. Angus, L. *et al.* The genomic landscape of metastatic breast cancer highlights changes in
708 mutation and signature frequencies. *Nat Genet* **51**, 1450-1458 (2019).
709 56. Motzer, R.J. *et al.* Nivolumab plus Ipilimumab versus Sunitinib in Advanced Renal-Cell
710 Carcinoma. *N Engl J Med* **378**, 1277-1290 (2018).
711 57. Motzer, R.J. *et al.* Survival outcomes and independent response assessment with nivolumab plus
712 ipilimumab versus sunitinib in patients with advanced renal cell carcinoma: 42-month follow-up
713 of a randomized phase 3 clinical trial. *J Immunother Cancer* **8**(2020).
714 58. Motzer, R.J. *et al.* Final Overall Survival and Molecular Analysis in IMmotion151, a Phase 3 Trial
715 Comparing Atezolizumab Plus Bevacizumab vs Sunitinib in Patients With Previously Untreated
716 Metastatic Renal Cell Carcinoma. *JAMA Oncol* (2021).
717 59. Epaillard, N. *et al.* BIONIKK: A phase 2 biomarker driven trial with nivolumab and ipilimumab or
718 VEGFR tyrosine kinase inhibitor (TKI) in naive metastatic kidney cancer. *Bull Cancer* **107**, eS22-
719 eS27 (2020).
720 60. Choueiri, T.K. & Kaelin, W.G., Jr. Targeting the HIF2-VEGF axis in renal cell carcinoma. *Nat Med*
721 **26**, 1519-1530 (2020).
722 61. van der Veldt, A.A. *et al.* Sunitinib for treatment of advanced renal cell cancer: primary tumor
723 response. *Clin Cancer Res* **14**, 2431-6 (2008).

62. Jonasch, E. *et al.* Belzutifan for Renal Cell Carcinoma in von Hippel-Lindau Disease. *N Engl J Med* **385**, 2036-2046 (2021).
63. Nyk, L. *et al.* Interobserver Variability in Assessment of Renal Mass Biopsies. *Urol J* **18**, 400-403 (2020).
64. Haas, M. Donor kidney biopsies: pathology matters, and so does the pathologist. *Kidney Int* **85**, 1016-9 (2014).
65. Osunkoya, A.O., Young, A.N., Wang, W., Netto, G.J. & Epstein, J.I. Comparison of gene expression profiles in tubulocystic carcinoma and collecting duct carcinoma of the kidney. *Am J Surg Pathol* **33**, 1103-6 (2009).
66. Casparie, M. *et al.* Pathology databanking and biobanking in The Netherlands, a central role for PALGA, the nationwide histopathology and cytopathology data network and archive. *Cell Oncol* **29**, 19-24 (2007).
67. Vasimuddin, M., Misra, S., Li, H. & Aluru, S. Efficient Architecture-Aware Acceleration of BWA-MEM for Multicore Systems,. *2019 IEEE International Parallel and Distributed Processing Symposium (IPDPS)* 314-324 (2019).
68. Cameron, D.L. *et al.* GRIDSS, PURPLE, LINX: Unscrambling the tumor genome via integrated analysis of structural variation and copy number. *bioRxiv*, 781013 (2019).
69. Karczewski, K.J. *et al.* The mutational constraint spectrum quantified from variation in 141,456 humans. *Nature* **581**, 434-443 (2020).
70. McLaren, W. *et al.* The Ensembl Variant Effect Predictor. *Genome Biology* **17**, 122 (2016).
71. Mermel, C.H. *et al.* GISTIC2.0 facilitates sensitive and confident localization of the targets of focal somatic copy-number alteration in human cancers. *Genome Biology* **12**, R41 (2011).
72. Martincorena, I. *et al.* Universal Patterns of Selection in Cancer and Somatic Tissues. *Cell* **171**, 1029-1041 e21 (2017).
73. Blokzijl, F., Janssen, R., van Boxtel, R. & Cuppen, E. MutationalPatterns: comprehensive genome-wide analysis of mutational processes. *Genome Medicine* **10**, 33 (2018).
74. Alexandrov, L.B. *et al.* The repertoire of mutational signatures in human cancer. *Nature* **578**, 94-101 (2020).
75. Cortés-Ciriano, I. *et al.* Comprehensive analysis of chromothripsis in 2,658 human cancers using whole-genome sequencing. *Nature Genetics* **52**, 331-341 (2020).
76. Debyani, C. *et al.* OncoKB: A Precision Oncology Knowledge Base. *JCO Precision Oncology*, 1-16 (2017).
77. Griffith, M. *et al.* CIViC is a community knowledgebase for expert crowdsourcing the clinical interpretation of variants in cancer. *Nature Genetics* **49**, 170-174 (2017).
78. Tamborero, D. *et al.* Cancer Genome Interpreter annotates the biological and clinical relevance of tumor alterations. *Genome Medicine* **10**, 25 (2018).
79. College ter Beoordeling van Geneesmiddelen. https://www.cbg-meb.nl/.
80. Landrum, M.J. *et al.* ClinVar: improvements to accessing data. *Nucleic Acids Research* **48**, D835-D844 (2019).
81. Dobin, A. *et al.* STAR: ultrafast universal RNA-seq aligner. *Bioinformatics* **29**, 15-21 (2012).
82. Yates, A.D. *et al.* Ensembl 2020. *Nucleic Acids Research* **48**, D682-D688 (2019).
83. Love, M.I., Huber, W. & Anders, S. Moderated estimation of fold change and dispersion for RNA-seq data with DESeq2. *Genome Biology* **15**, 550 (2014).
84. Korotkevich, G. *et al.* Fast gene set enrichment analysis. *bioRxiv*, 060012 (2021).
85. Liberzon, A. *et al.* The Molecular Signatures Database (MSigDB) hallmark gene set collection. *Cell Syst* **1**, 417-425 (2015).

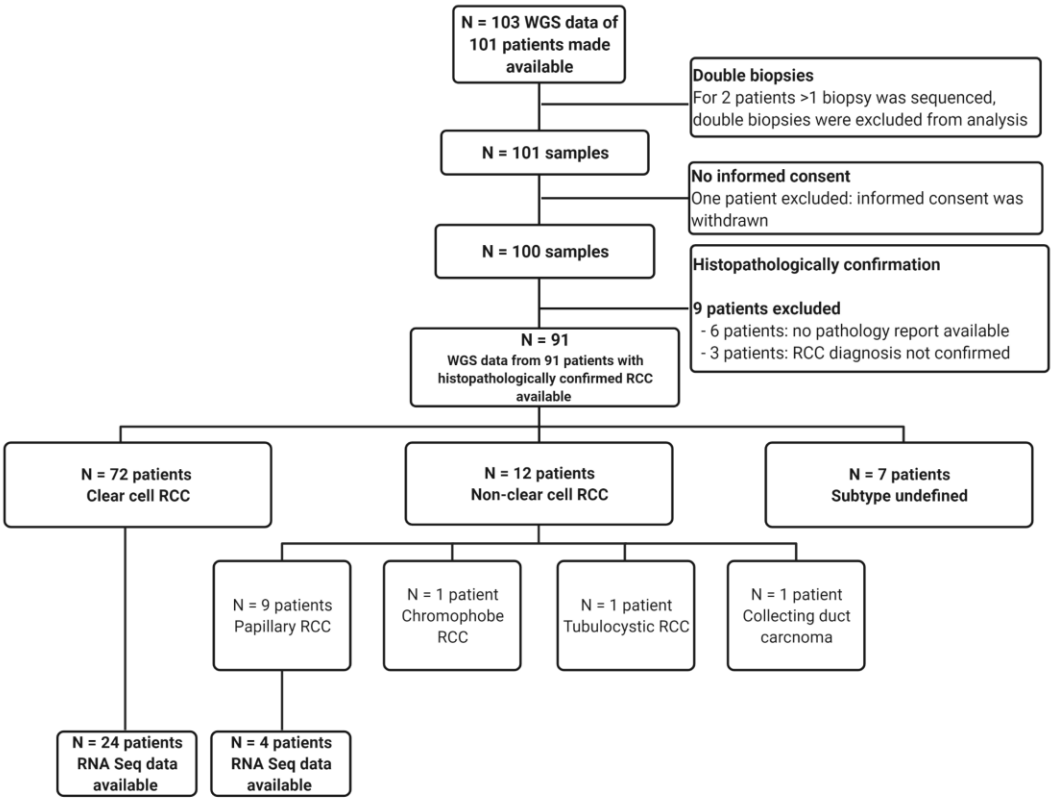
N = 103 WGS data of 101 patients made available
Double biopsies
For 2 patients >1 biopsy was sequenced, double biopsies were excluded from analysis
N = 101 samples
No informed consent
One patient excluded: informed consent was withdrawn
N = 100 samples
Histopathologically confirmation
9 patients excluded
- 6 patients: no pathology report available
- 3 patients: RCC diagnosis not confirmed
N = 91
WGS data from 91 patients with histopathologically confirmed RCC available
N = 72 patients
Clear cell RCC
N = 12 patients
Non-clear cell RCC
N = 7 patients
Subtype undefined
N = 9 patients
Papillary RCC
N = 1 patient
Chromophobe RCC
N = 1 patient
Tubulocystic RCC
N = 1 patient
Collecting duct carcnoma
N = 24 patients
RNA Seq data available
N = 4 patients
RNA Seq data available

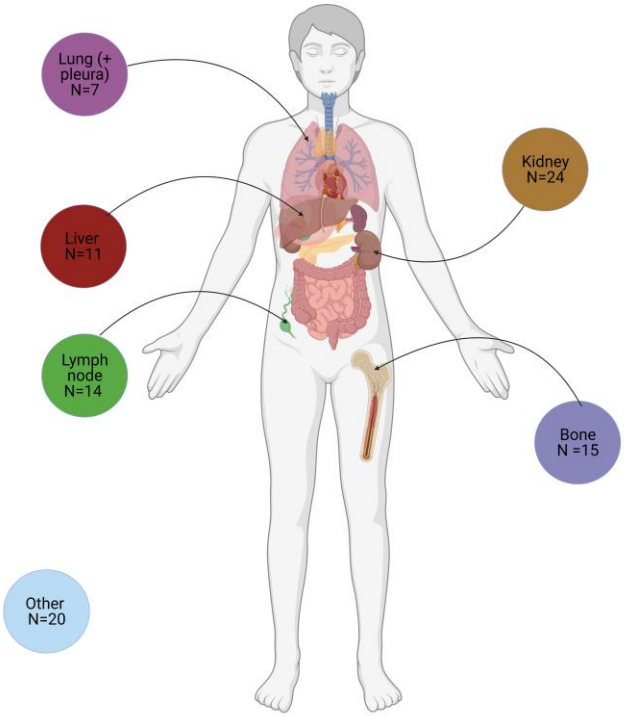
Lung (+ pleura) N=7
Liver N=11
Lymph node N=14
Other N=20
Kidney N=24
Bone N =15

A
ccRCC
pRCC
Undefined Subtype
chRCC
CDC
tRCC
Mutations per Mb (Genome-wide TMB; log10)
50.0
25.0
10.0
5.0
2.5
0.0
Mutational categories
High TMB (≥10)
Medium TMB (≥5-10)
Low TMB (0-5)
B
Mean genome-wide ploidy
Mean genome-wide ploidy
0 1 2 3 4 5
C
Structural variants
2500
1000
500
250
0
D
Relative frequency
100%
75%
50%
25%
0%
Structural variant categories
Deletions
Tandem Duplications
Inversions
Translocations
Break-ends
Insertions
E
Mut. Signatures (Genome-wide)
Mutational Signatures (COSMIC v3.1)
Spontaneous deamination of 5-methylcytosine (clock-like signature) (SBS1)
Activity of APOBEC family of cytidine deaminases (SBS2, SBS13)
Defective homologous recombination DNA damage repair (SBS3, ID6)
Tobacco smoking (SBS4, ID3, SBS94)
Unknown (clock-like signature) (SBS5)
Defective DNA mismatch repair (>4 signatures)
Ultraviolet light exposure (>4 signatures)
Polimerase eta somatic hypermutation activity (SBS9)
Defective POLD1 proofreading (SBS10c)
Damage by reactive oxygen species (SBS18)
Aristolochic acid exposure (SBS22)
Chemotherapy treatment (SBS25)
Tobacco chewing (SBS29)
Azathioprine treatment (SBS32)
Defective DNA base excision repair due to MUTYH mutations (SBS36)
Unknown (SBS40)
Haloalkane exposure (SBS42)
Indirect effects of activation-induced cytidine deaminase (AID) (SBS85)
Unknown chemotherapy treatment (SBS86)
Unknown (>4 signatures)
Filtered (<5%)
F
Relative Frequency
Mutational Changes (SNV)
C>A
C>G
C>T
T>A
T>C
T>G
G
Chromothripsis
H
Treatment Naive
Treatment Naive
Yes
No
I
Treatment
First treatment after biopsy
TKI
Immunotherapy
Immunotherapy combination
Immunotherapy + TKI
J
RECIST
RECIST v1.1 - First Response
PR
SD
PD
NA

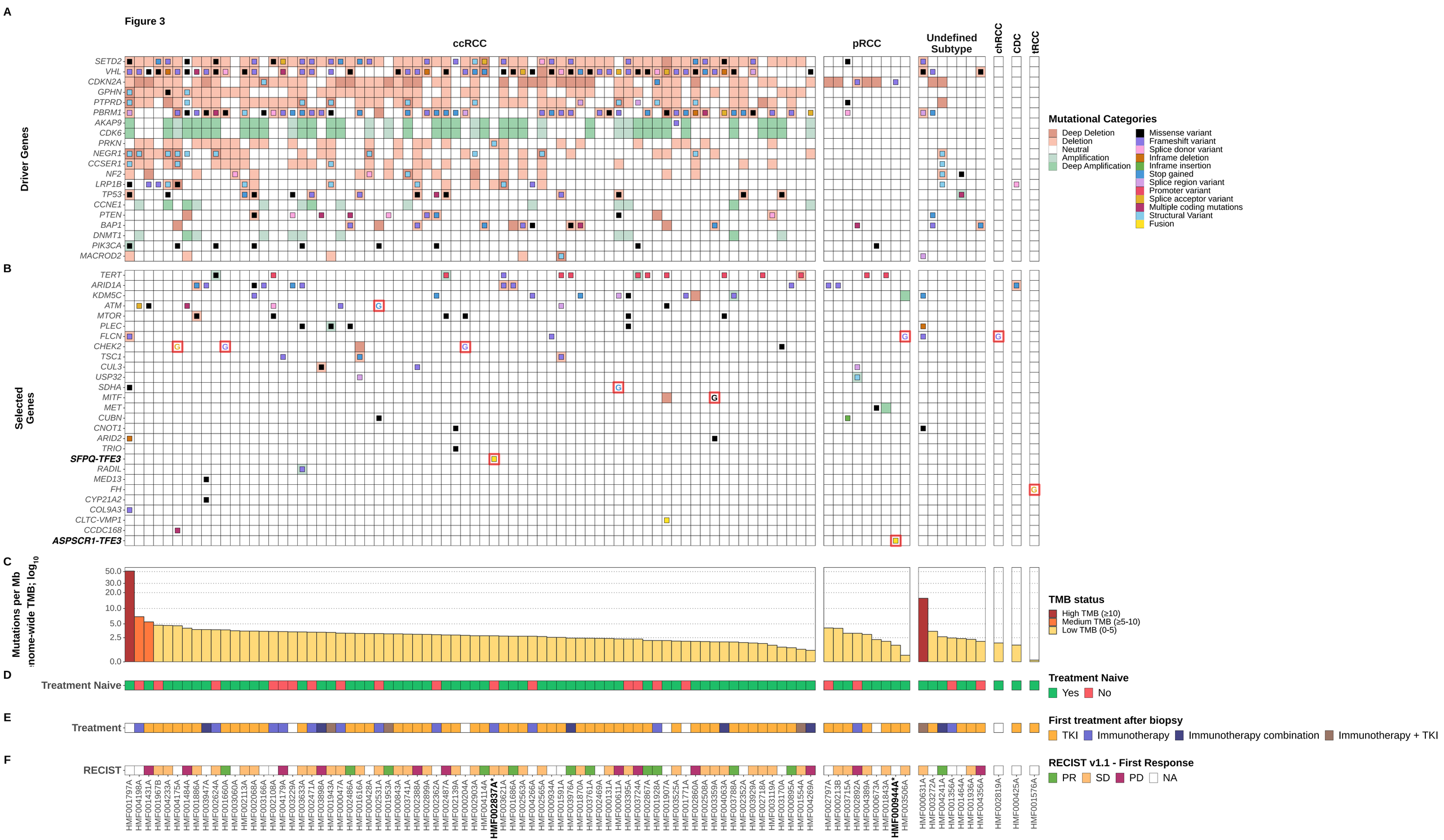
Figure 3
A
ccRCC
pRCC
Undefined Subtype
chRCC
CDC
tRCC
Driver Genes
SETD2
VHL
CDKN2A
GPHN
PTPRD
PBRM1
AKAP9
CDK6
PRKN
NEGR1
CCSER1
NF2
LRP1B
TP53
CCNE1
PTEN
BAP1
DNMT1
PIK3CA
MACROD2
Mutational Categories
Deep Deletion
Deletion
Neutral
Amplification
Deep Amplification
Missense variant
Frameshift variant
Splice donor variant
Inframe deletion
Inframe insertion
Stop gained
Splice region variant
Promoter variant
Splice acceptor variant
Multiple coding mutations
Structural Variant
Fusion
B
Selected Genes
TERT
ARID1A
KDM5C
ATM
MTOR
PLEC
FLCN
CHEK2
TSC1
CUL3
USP32
SDHA
MITF
MET
CUBN
CNOT1
ARID2
TRIO
SFPQ-TFE3
RADIL
MED13
FH
CYP21A2
COL9A3
CLTC-VMP1
CCDC168
ASPSCR1-TFE3
C
Mutations per Mb
Genome-wide TMB; log10
50.0
30.0
20.0
10.0
5.0
2.5
0.0
TMB status
High TMB (≥10)
Medium TMB (≥5-10)
Low TMB (0-5)
D
Treatment Naive
Treatment Naive
Yes
No
E
Treatment
First treatment after biopsy
TKI
Immunotherapy
Immunotherapy combination
Immunotherapy + TKI
F
RECIST
RECIST v1.1 - First Response
PR
SD
PD
NA
HMF001797A
HMF004198A
HMF001431A
HMF001967B
HMF004233A
HMF004175A
HMF001484A
HMF001886A
HMF003947A
HMF002624A
HMF001660A
HMF003060A
HMF002113A
HMF002068A
HMF003166A
HMF002108A
HMF004179A
HMF003229A
HMF003633A
HMF002471A
HMF003898A
HMF001943A
HMF000047A
HMF002486A
HMF001616A
HMF000428A
HMF002531A
HMF001953A
HMF000843A
HMF003741A
HMF002388A
HMF002899A
HMF002362A
HMF002487A
HMF002139A
HMF000204A
HMF002903A
HMF004114A
HMF002837A*
HMF003621A
HMF001686A
HMF002563A
HMF004266A
HMF002565A
HMF000934A
HMF001591A
HMF003976A
HMF001870A
HMF003761A
HMF002469A
HMF000131A
HMF000611A
HMF003395A
HMF003724A
HMF002867A
HMF001928A
HMF001907A
HMF003525A
HMF001771A
HMF002860A
HMF002508A
HMF003359A
HMF004063A
HMF003788A
HMF002352A
HMF003929A
HMF002718A
HMF003119A
HMF003170A
HMF000895A
HMF001554A
HMF004269A
HMF002797A
HMF000213B
HMF003715A
HMF002892A
HMF004389A
HMF000673A
HMF001843A
HMF000944A*
HMF003506A
HMF000631A
HMF003272A
HMF004241A
HMF001356A
HMF001464A
HMF001936A
HMF004356A
HMF002819A
HMF000425A
HMF001576A

Actionable targets

iClusion Data

A

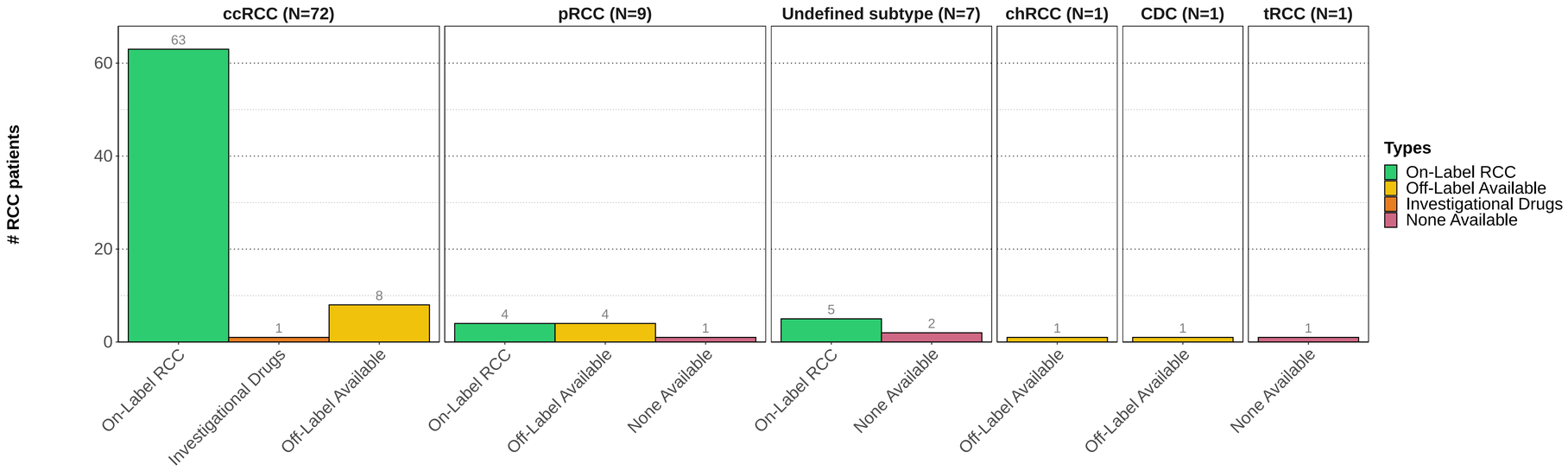

B

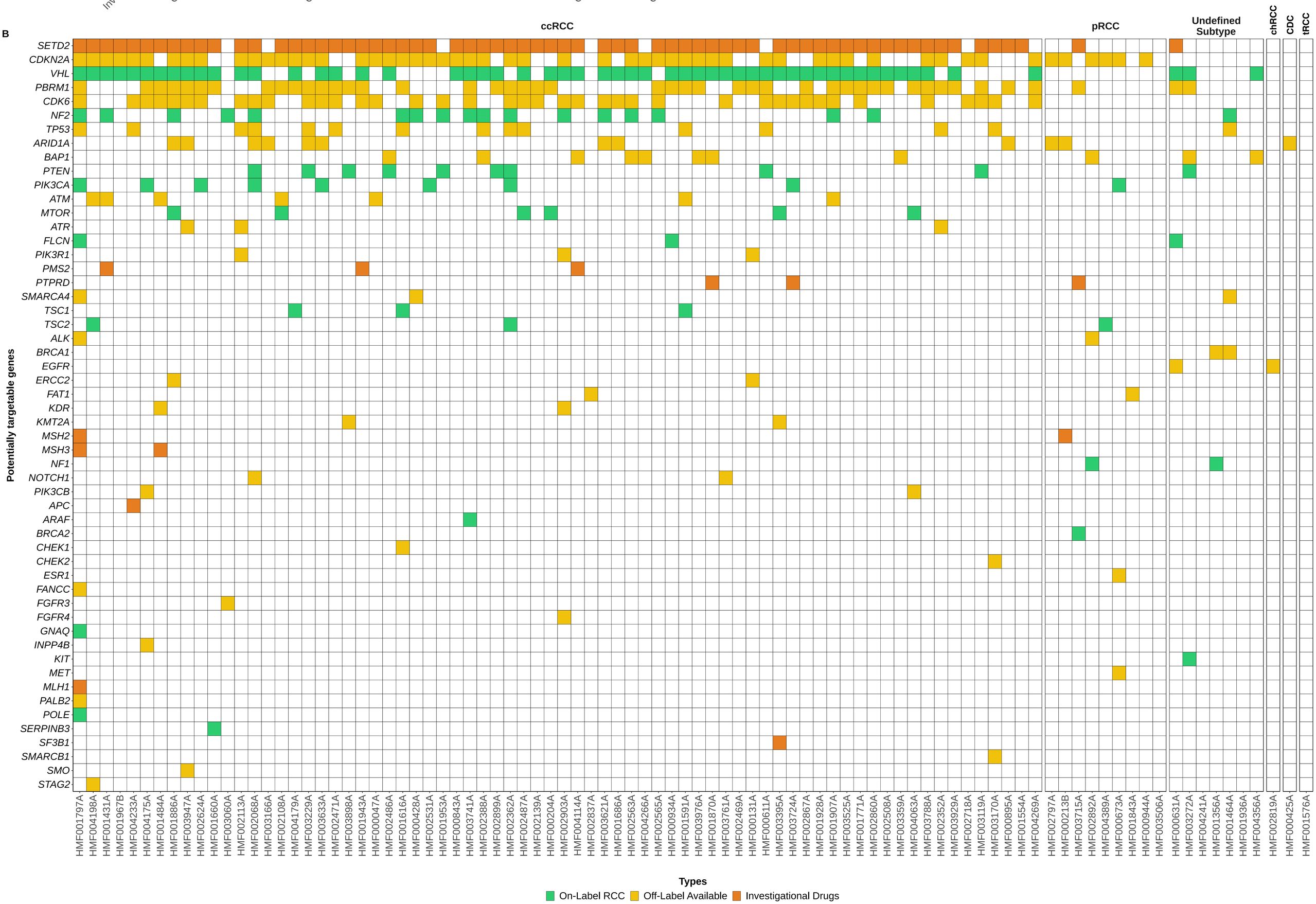

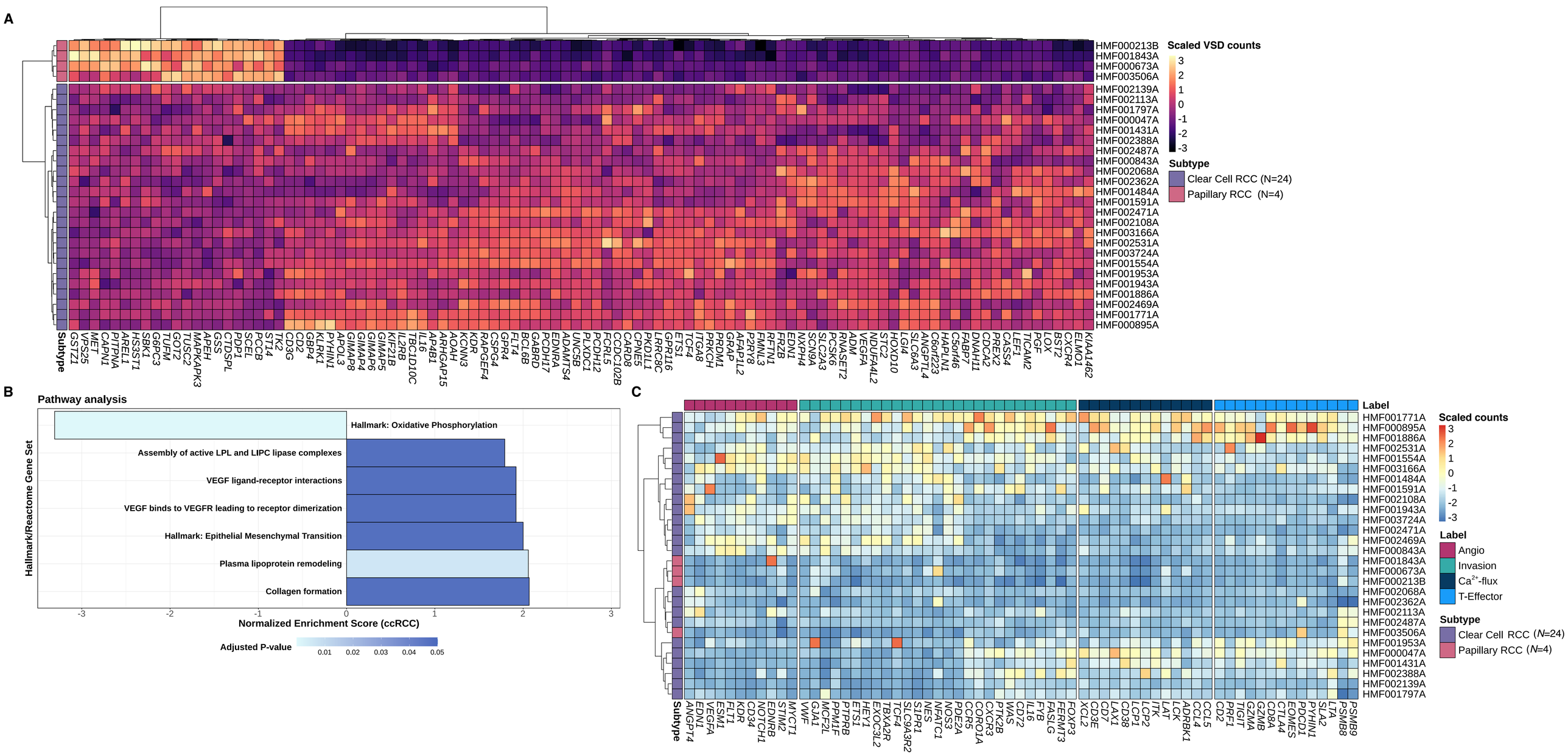
A
Scaled VSD counts
3
2
1
0
-1
-2
-3
Subtype
Clear Cell RCC (N=24)
Papillary RCC (N=4)
HMF000213B
HMF001843A
HMF000673A
HMF003506A
HMF002139A
HMF002113A
HMF001797A
HMF000047A
HMF001431A
HMF002388A
HMF002487A
HMF000843A
HMF002068A
HMF002362A
HMF001484A
HMF001591A
HMF002471A
HMF002108A
HMF003166A
HMF002531A
HMF003724A
HMF001554A
HMF001953A
HMF001943A
HMF001886A
HMF002469A
HMF001771A
HMF000895A
Subtype
GST21 VPS25 MET CAPN1 PITPNA AREL1 HS3ST1 SBK1 G6PC3 TUFM GOT2 TUSC2 MAPKAPK3 APEH GSS CTDSPL PDP1 SCEL PCCB ST14 TK2 CD3G CD2 GBP4 KLRK1 PYHIN1 APOL3 GIMAP8 GIMAP4 GIMAP6 GIMAP5 KIF21B IL2RB TBC1D10C IL16 AP4B1 ARHGAP15 AOAH KCNN3 KDR RAPGEF4 CSPG4 GPR4 FLT4 BCL6B GABRD PCDH17 EDNRA ADAMTS4 UNC5B PLXDC1 PCDH12 FCRL5 CCDC102B CARD8 CPNE5 PKD1L1 LRRC8C GPR116 ETS1 TCF4 ITGA8 PRKCH PRDM1 GRAP AFAP1L2 P2RY8 FMNL3 RFTN1 FRZB EDN1 NXPH4 SCN9A SLC2A3 PCSK6 RNASET2 VEGFA ADM NDUFA4L2 STC2 HOXD10 LGI4 SLC6A3 ANGPTL4 C6orf223 HAPLN1 C5orf46 FABP7 DNAH11 CDCA2 PREX2 CASS4 LEF1 TICAM2 PGF LOX BST2 CXCR4 ELMO1 KIAA1462
B
Pathway analysis
Hallmark/Reactome Gene Set
Hallmark: Oxidative Phosphorylation
Assembly of active LPL and LIPC lipase complexes
VEGF ligand-receptor interactions
VEGF binds to VEGFR leading to receptor dimerization
Hallmark: Epithelial Mesenchymal Transition
Plasma lipoprotein remodeling
Collagen formation
-3 -2 -1 0 1 2 3
Normalized Enrichment Score (ccRCC)
Adjusted P-value
0.01 0.02 0.03 0.04 0.05
C
Label
Scaled counts
3
2
1
0
-1
-2
-3
Label
Angio
Invasion
Ca2+-flux
T-Effector
Subtype
Clear Cell RCC (N=24)
Papillary RCC (N=4)
HMF001771A
HMF000895A
HMF001886A
HMF002531A
HMF001554A
HMF003166A
HMF001484A
HMF001591A
HMF002108A
HMF001943A
HMF003724A
HMF002471A
HMF002469A
HMF000843A
HMF001843A
HMF000673A
HMF000213B
HMF002068A
HMF002362A
HMF002113A
HMF002487A
HMF003506A
HMF001953A
HMF000047A
HMF001431A
HMF002388A
HMF002139A
HMF001797A
Subtype
ANGPT4 EDN1 VEGFA ESM1 FLT1 KDR CD34 NOTCH1 EDNRB STM2 MYCT1 VWF GJA1 MCF2L PPM1F PTPRB ETS1 HEY1 EXOC3L2 TBXA2R TCF4 SLC9A3R2 S1PR1 NES NFATC1 NOS3 PDE2A CCR5 CORO1A CXCR3 PTK2B WAS CD72 IL16 FYB FASLG FERMT3 FOXP3 XCL2 CD3E CD7 LAX1 CD38 LCP1 LCP2 ITK LAT LCK ADRBK1 CCL4 CCL5 CD2 PRF1 TIGIT GZMA GZMB CD8A CTLA4 EOMES PDCD1 PYHIN1 SLA2 LTA PSMB8 PSMB9